Int. J. Electrochem. Sci., 17 **(2022)** Article Number: 220522, doi: 10.20964/2022.05.31

International Journal of
ELECTROCHEMICAL
SCIENCE
www.electrochemsci.org

Growth Mechanisms and Properties of DC Electrodeposited Ni-Co/hBN Composite Coatings Prepared on Q235 Steel

Zengxiong Ruan, Xuewei Zhu[*]*, Xiaofeng Wei*[*]*, Yuchen Wu, Menglei Ma, Tongtong Wu*

Department of Mechanical Engineering, College of Mechanical and Electronic engineering, Northwest A & F University, Yangling, Shaanxi, China
[*]E-mail: zxw_83614@163.com
[*]E-mail: wxf8412@nwsuaf.edu.cn

Received: 20 January 2022 / *Accepted:* 23 February 2022 / *Published:* 5 April 2022

In this paper, a Ni-Co/hBN (hexagonal boron nitride) composite coating using hBN included in Ni-Co alloy coatings was prepared by DC electrodeposition. The effects of Co and hBN particles on the surface morphology, composition, grain size and hardness of the composites were investigated by X-ray diffraction (XRD), energy dispersive X-ray analysis (EDS), scanning electron microscopy (SEM) and Vickers microhardness testing. Potentiodynamic polarization was adopted to study the corrosion behavior of the coatings, and the corrosive medium was a 3.5 wt% NaCl solution. As the Co content increased, the surface morphology of the Ni-Co/hBN composite coatings gradually changed from pyramidal to spherical. Due to the addition of Co and hBN, the crystalline size of the coatings was reduced from 86 nm to 24 nm, and the microhardness was increased from 220 HV to 575 HV. The electrochemical analysis results showed that the addition of Co and hBN enhanced the corrosion resistance properties of the coatings. Among the coatings studied, the corrosion current density of the Ni-37Co/hBN composite coating was 14 times lower than that of the Ni/hBN composite coating, which was 0.645 μAcm^{-2}.

Keywords: composite coatings; corrosion resistance; electrodeposition; hBN particles; Ni-Co alloy

1. INTRODUCTION

The corrosion of metals is common in daily life, and the corrosion of metal products will affect the safety and reliability of the metal structure or even scrap. The corrosion of metal materials will cause a serious waste of resources, affect the accuracy of products, shorten the service life of metal products, and cause extremely serious economic losses [1]. There are extremely high requirements for corrosion resistance of metal materials in the machinery, metallurgy, electronics, aerospace and chemical industries [2, 3].

Surface engineering technology is an important method for reducing the corrosion of metal materials and mainly includes thermal spraying, surfacing, electroplating, chemical plating and vapor deposition [4]. Electroplating has become an important industrial technology for preparing anticorrosion coatings due to its moderate cost, high efficiency, mass production, and lack of a high-temperature and high-pressure environment [5, 6].

Pure Ni coatings are widely used in the microelectronics industry due to their good magnetic properties and corrosion resistance [7]. However, Ni also has disadvantages such as low hardness and poor wear resistance. Therefore, binary or multiple nickel-based alloy coatings have been gradually developed to expand their application range, such as Ni-W [8], Ni-Mo [9], Ni-Co [10], Ni-Cr [11], Ni-Cu [12] and Ni-Cr-Mo [13]. Ni-Co alloy coatings have many excellent physical, chemical and mechanical properties, so they are widely used in electroforming, protective decorative coatings, cathodic hydrogen evolution materials and other fields [14-18].

The composite coating prepared by adding unique particles to the Ni-Co alloy coating can greatly improve its corrosion resistance and wear resistance [19-22]. It was found that the incorporation of nanoparticles improves the performance of the composite coating compared with the incorporation of microparticles [23-29]. hBN is an inorganic material that has high temperature stability, low thermal expansion, high corrosion resistance, good thermal shock resistance, high electrical resistance and insulating properties, and is nonabrasive and chemically inert [30]. The composite coating prepared by adding hBN to the Ni-based alloy has good corrosion resistance and wear resistance. There are few studies of the effect on the performance of Ni-Co alloy coatings by adding hBN to them.

The main purpose of this paper is to report the preparation of Ni-Co/hBN nanocomposite coatings on Q235 steel by DC electroplating, mainly to study the influence of bath composition on the corrosion resistance and chemical composition of the composite coatings.

2. EXPERIMENTAL

2.1 Coating preparation

The bath compositions and deposition parameters are shown in Table 1. They are based on a Watt plating solution. All of the chemicals were purchased from Sinopharm Chemical Reagent Co., Ltd. (Shanghai, China). The hBN powder was purchased from Chaowei Nano Technology Co., Ltd. (Shanghai, China). The cathode was a Q235 steel plate, which contained Fe and the microelements C, Mn, Si, S and P. The anode was a pure nickel plate. Both were produced by Jilong Metal Materials Co., Ltd. (Shenzhen, China). The morphology of the hBN nanoparticles is shown in Figure 1. The particle size is approximately 50 nm in the form of flakes. Before electroplating, Q235 steel was subjected to pretreatment processes such as grinding, polishing, degreasing, activation, and water washing. The surface of the substrate was ground to smooth with 220-2000# sandpaper in sequence until there were no defects, such as pores, around it. Afterwards, it was polished with abrasive paste to obtain a smooth and flat sample surface. It was degreased with acetone, activated in dilute hydrochloric acid for 15 s, and then rinsed with deionized water. A 250 mL glass beaker was used as the bath. The experimental

chemicals were accurately weighed by an electronic analytical balance, then dissolved in deionized water and diluted to the required volume of 250 ml of plating solution. To uniformly disperse hBN particles in the plating solution, magnetic stirring and ultrasonic stirring were used for alternating stirring for 24 hours. The pH value of the plating bath was adjusted to 4 with dilute hydrochloric acid and sodium hydroxide.

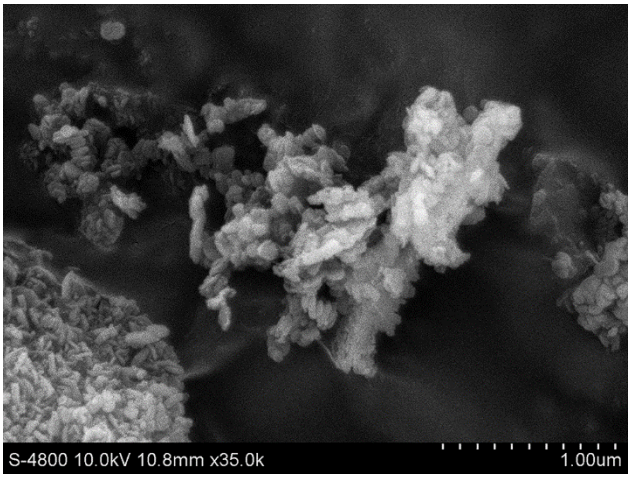

Figure 1. SEM image of hBN nanoparticles

Table 1. Bath compositions and operating conditions

Plating bath	Parameters (g/L)
$NiSO_4 \cdot 6H_2O$	250
$NiCl_2 \cdot 6H_2O$	30
$CoSO_4 \cdot 7H_2O$	0–50
$C_{12}H_{25}SO_4Na$ (SDS)	0.1
H_3BO_3	35
hBN powder size	50 (nm)
Current density	1–5 A/dm^2
Temperature	60 ℃
Current type	DC
pH	4
hBN	1–9

Electrochemical deposition was carried out with an NP360W DC stabilized power supply (Guce Electronic Technology Co., Ltd, Shenzhen, China) with a plating time of 40 min. After the electrodeposition process, the surface was cleaned with deionized water and then dried. The Ni-Co/hBN composite coatings prepared with different cobalt sulfate concentrations (0, 10, 20, 30, 40, 50 g/L) plating solutions at 3 A/dm^2 and 5 g/L hBN are shown in Table 2 (other bath compositions and operating conditions are shown in Table 1). The number in the name of the coatings represents the Co content in the coatings (Ni-17Co/hBN contained 17 wt% Co content in the coating).

Table 2. Coatings prepared under different cobalt sulfate concentrations

Cobalt sulfate concentration (g/L)	Co content (wt.%)	Coatings
0	0	Ni/hBN
10	17	Ni-17Co/hBN
20	32	Ni-32Co/hBN
30	37	Ni-37Co/hBN
40	40	Ni-40Co/hBN
50	53	Ni-53Co/hBN

2.2 Characterization and electrochemical testing

The surface morphology and element content of the prepared coatings were observed by a Nova Nano SEM-450 scanning electron microscope coupled with an energy dispersive X-ray spectrometer developed by the FEI Company in the USA. The phase structure of the coatings was determined by a D8 ADVANCE A25 X-ray diffractometer with CuKα radiation (Bruker, Germany), which was operated at 40 kilovolts and 40 milliamperes. The Debye-Scherrer equation was used to calculate the average grain size of the composite coatings:

$$D = \frac{0.9\lambda}{\beta \cos\theta} \quad (1)$$

Where θ is the peak diffraction angle, λ is the X-ray beam wavelength (λ= 1.5406 Å), D is the average crystal grain size of the coatings, and β is the angular breadth of the diffraction peak at half height (FWHM). The microhardness was determined by using an HV-1000AT microhardness tester (Aolongxingdi Testing Equipment Co., Ltd., Shanghai, China) at an applied load of 50 g for 10 s. An average of five different measurements was used as the resultant microhardness value. The polarization curve of the composite coatings was tested by a CHI1660E electrochemical workstation (Chenhua Instrument Co., Ltd., Shanghai, China). Potentiodynamic polarization testing was performed in a 3.5% NaCl solution at room temperature (25 ℃) and without stirring. A three-electrode cell was adopted in the electrochemical test. The reference electrode was a saturated calomel electrode (SCE), the counter electrode was a platinum sheet, and the working electrode was a sample coating. The plating parts were immersed in the solution for 60 minutes before testing to obtain the open circuit potential (Eocp). The dynamic scanning was swept in the range of ±250 mV relative to the Eocp with a scan rate of 1 mV/s. The corrosion current density was calculated by the Stern-Geary equation.

3. RESULTS AND DISCUSSION

3.1 Coatings composition

The black curve in Figure 2 shows the influence of current density on the hBN content in the coatings deposited at 30 g/L cobalt sulfate and 5 g/L hBN (other bath compositions and operating conditions are shown in Table 1). When the current density increases from 1 A/dm^2 to 3 A/dm^2, the hBN content increases from 2.4 wt% to 5.9 wt%, and when the current density continuously increases to 5

A/dm^2, the hBN content is finally reduced to 2.3 wt%. It is worth noting that the hBN content reaches the highest value of 5.9 wt% when the current density is 3 A/dm^2.

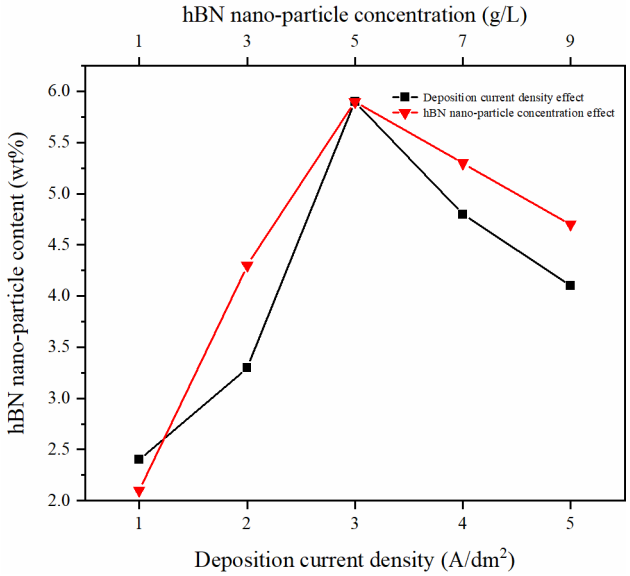

Figure 2. Effect of hBN nanoparticle concentration and deposition current density on the hBN nanoparticle content in the Ni-Co/hBN nanocomposite coatings

The change in hBN nanoparticle content versus the current density is caused by the relative magnitudes of the incorporation rate of hBN particles and the reduction rate of metal cations in the plating solution [31]. When the current density is lower than a certain value, the reduction rate of metal cations in the plating solution is greater than the incorporation rate of hBN particles, so the hBN particle content is lower. With the continuous increase in current density, the reduction rate of metal cations drops behind the incorporation rate of hBN particles, which increases the hBN content in the coating, reaching a maximum value of 5.9 wt% when the current density is 3 A/dm^2. However, the hBN incorporation rate drops behind the reduction rate of metal cations again as the current density further increases. Therefore, the hBN content is reduced.

The change in hBN content versus the concentration of hBN in the bath is depicted by the red curve in Figure 2. This experiment was performed at a constant current density (3 A/dm^2) and cobalt sulfate concentration of 30 g/L (other bath compositions and operating conditions are shown in Table 1). The hBN content in the coatings first increases and then decreases as the hBN concentration increases. It reaches a maximum value of 5.9 wt% at 5 g/L. Since the size of the selected hBN particles is at the nanometer level, a high concentration of hBN particles in the bath will cause them to agglomerate and reduce the content of hBN in the coatings. Therefore, the highest value of hBN nanoparticle content in the coatings is reached at a concentration of 5 g/L hBN and a current density of 3 A/dm^2.

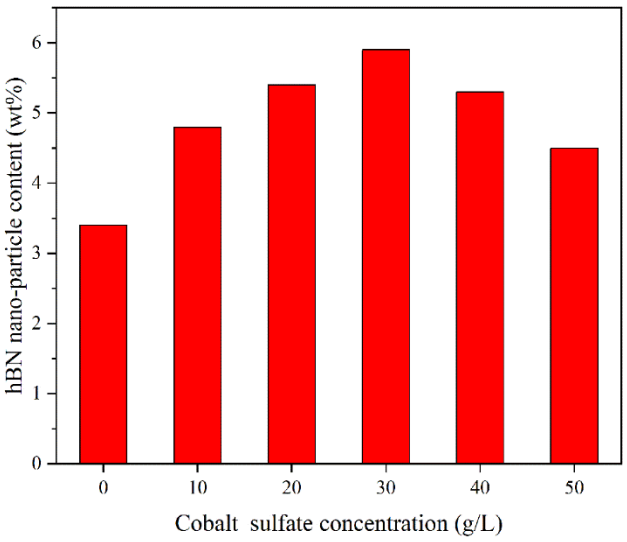

Figure 3. The hBN particle content in the Ni-Co/hBN nanocomposite coatings at different cobalt sulfate concentrations

As illustrated in Figure 3, the cobalt sulfate concentration has a significant effect on the hBN content (at 3 A/dm^2 and 5 g/L hBN). The content of hBN increases from 3.4 wt% to 5.9 wt% as the concentration of cobalt sulfate changes from 0 g/L to 30 g/L. Thereafter, the hBN content in the coating is reduced from 5.9 wt% to 4.5 wt% with a continuous increase in the cobalt sulfate concentration from 30 g/L to 50 g/L.

Properly increasing the cobalt sulfate concentration in the bath benefits an increase in the hBN content in the Ni-Co/hBN composite coatings. This is because Co^{2+} is more easily adsorbed on the hBN surface than is Ni^{2+} [32]. A decrease in the hBN particle content in the coating occurs because the hBN nanoparticles are saturated by metallic cations.

3.2 Surface morphology and phase structure

To study the effect of Co content on the surface morphology of Ni-Co/hBN composite coatings, SEM observation was used (Figure 4).

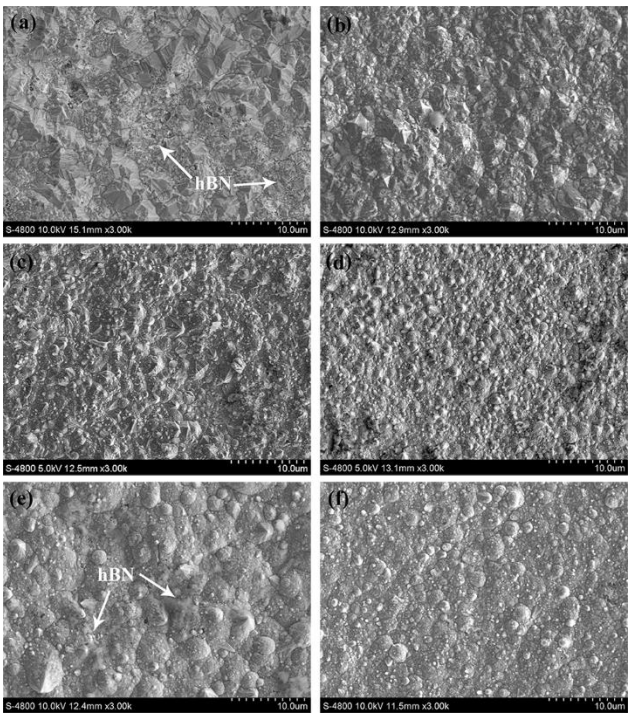

Figure 4. Surface morphologies of (a) Ni/hBN, (b) Ni-17Co/hBN, (c) Ni-32Co/hBN, (d) Ni-37Co/hBN, (e) Ni-40Co/hBN and (f) Ni-53Co/hBN nanocomposite coatings

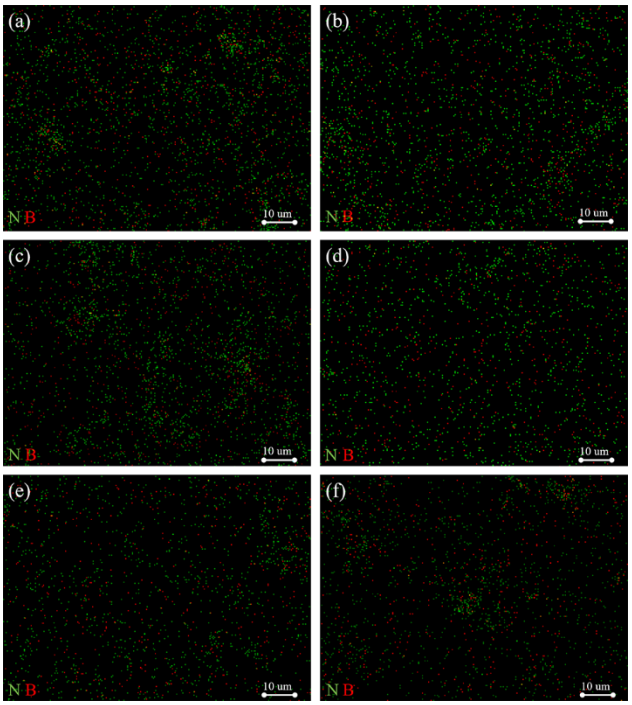

Figure 5. N and B dot-map patterns of (a) Ni/hBN, (b) Ni-17Co/hBN, (c) Ni-32Co/hBN, (d) Ni-37Co/hBN, (e) Ni-40Co/hBN and (f) Ni-53Co/hBN nanocomposite coatings

As the Co content increases from 0 wt% to 53 wt%, the surface morphology of the Ni-Co/hBN composite coatings changes gradually from pyramidal to spherical. The surface morphologies of the

Ni/hBN, Ni-17Co/hBN, Ni-32Co/hBN and Ni-37Co/hBN composite coatings are pyramidal and become denser and flatter as the Co content increases (Figure 4a-4d). This result can be explained by the increase in the concentration of cobalt sulfate in the electrolyte resulting in an increase in the Co and hBN nanoparticle contents in the coatings, which refines the structures of the coatings. Some spherical structures begin to appear in the Ni-40Co/hBN composite coating (Figure 4e), while the Ni-53Co/hBN composite coating is basically transformed into a spherical structure (Figure 4f). Studies have verified that the Co content can markedly change the microstructure of the Ni-Co coating. Hefnawy [17] reported that the incorporation of Co alters the morphology of the Ni-TiN coating to a denser structure. Bakhit [33] showed that spherical structures emerge when the Co content is 40 wt% in the Ni-Co coating.

Figure 5 illustrates N and B mapping images of the Ni-Co/hBN composite coatings with different Co contents. This result reveals that the hBN nanoparticles are homogeneously distributed in the coatings, which reduces the effective area of the matrix contacting the corrosive medium and enhances the corrosion resistance of the coatings.

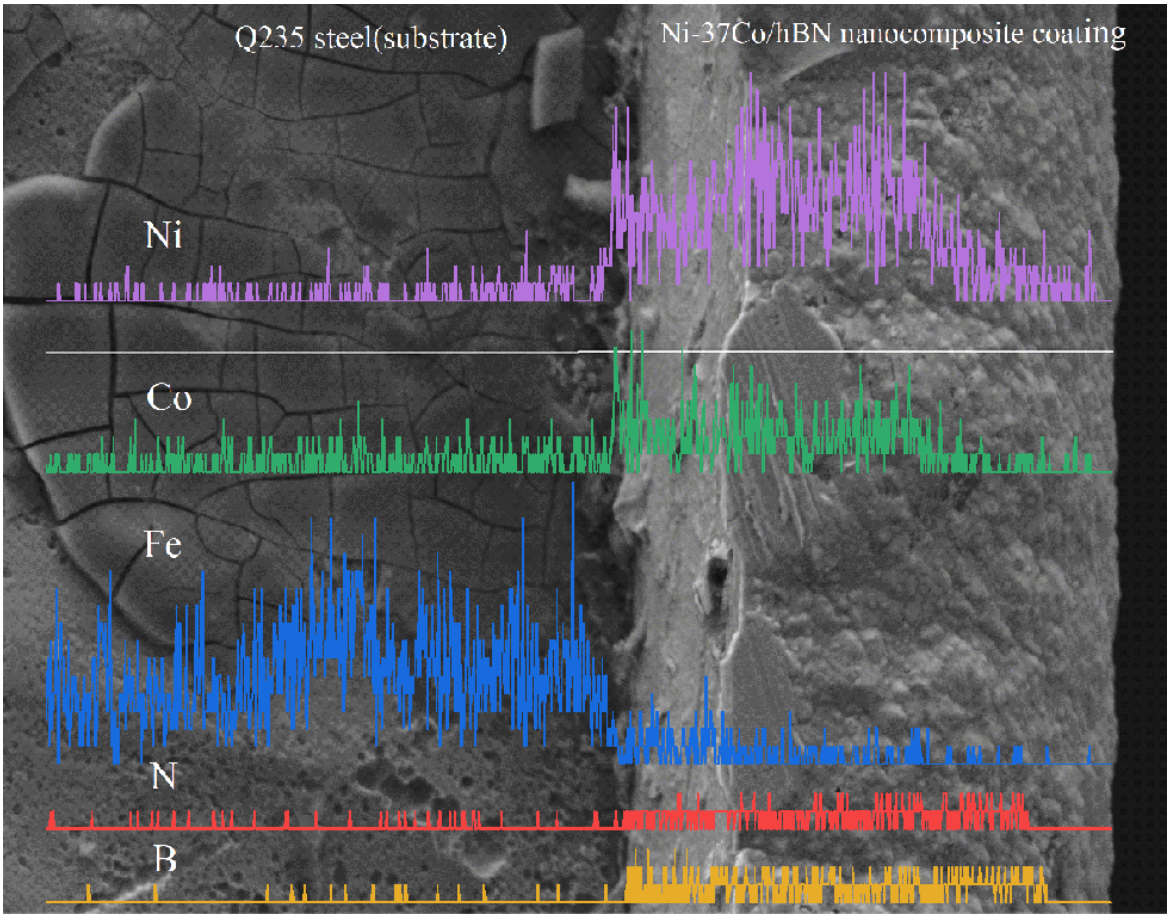

Figure 6. Line scans of the elements Co, Ni, N, B and Fe through the cross section of the Ni-37Co/hBN nanocomposite coating

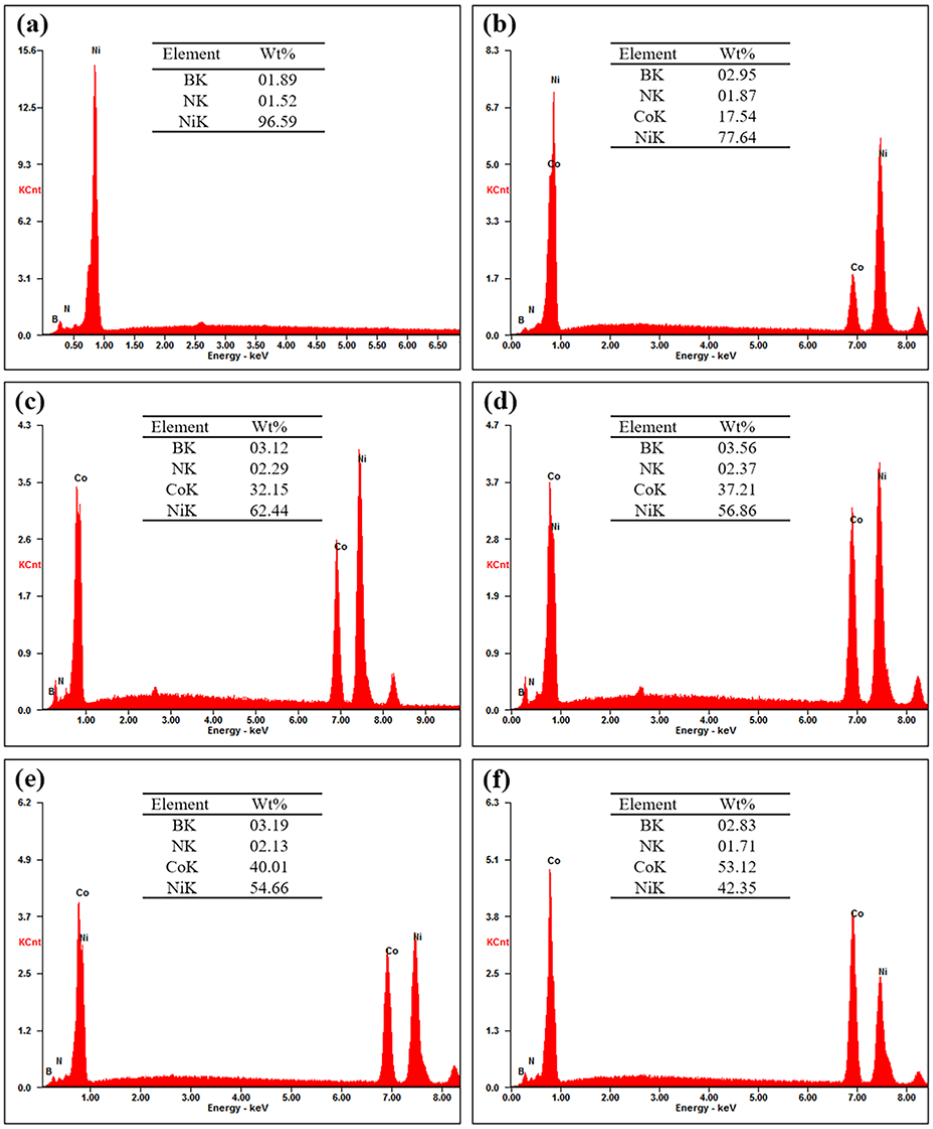

Figure 7. EDS spectra of (a) Ni/hBN, (b) Ni-17Co/hBN, (c) Ni-32Co/hBN, (d) Ni-37Co/hBN, (e) Ni-40Co/hBN and (f) Ni-53Co/hBN nanocomposite coatings

Thereafter, to investigate the composition distribution of the Ni-37Co/hBN composite coating, line scans of the elements Fe, Co, Ni, N and B are revealed on a cross-sectional SEM image (Figure 6). This result indicates uniformity of the hBN nanoparticle distribution in the coatings. The EDS spectra and elemental content of the nanocomposite coatings with different Co contents are shown in Figure 7. As the Co content increases, the contents of Co, B and N also increase. This indicates that the Co content and the amount of hBN nanoparticles in the Ni-Co/hBN composite coatings increase by increasing the cobalt sulfate concentration.

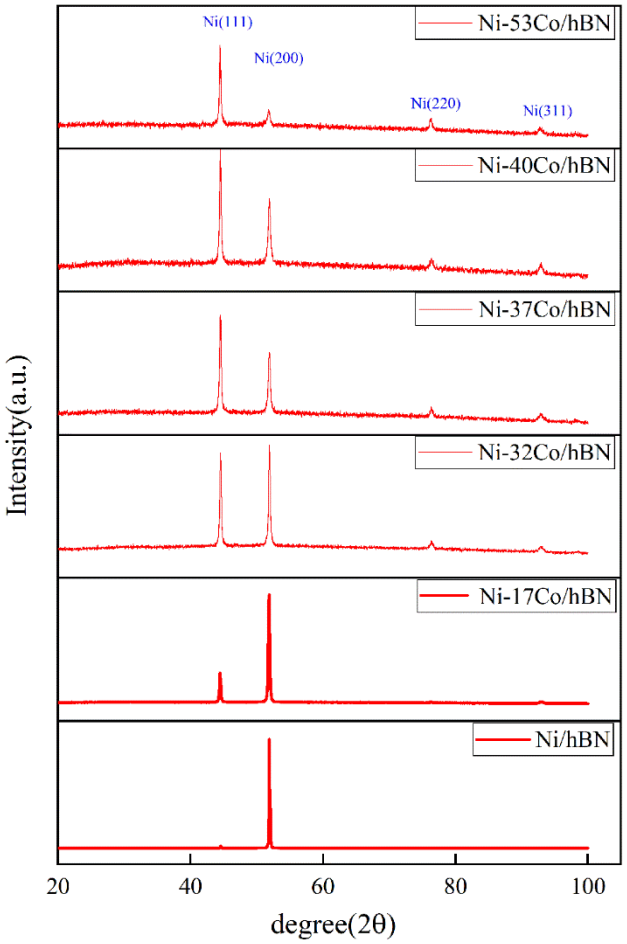

Figure 8. XRD patterns of Ni-Co/hBN nanocomposite coatings obtained with varying Co contents

Figure 8 depicts the XRD patterns deposited in baths containing varying cobalt sulfate concentrations of 0, 10, 20, 30, 40 and 50 g/L. There are four peaks in the XRD patterns of all the composite coatings, which correspond to Ni (111), (200), (220) and (311) diffraction peaks. The EDX analysis reflects that Co exists in the coatings, which confirms that Co replaces a part of the Ni lattices to form a Ni-Co solid solution. Although there are no considerable changes in the phase structure of the composite coatings, all of them are fcc structures, and the peak intensity changes significantly. As the Co content increases, the (111) diffraction peak intensity increases, while the (200) diffraction peak intensity decreases. This result is consistent with the previous literature as reported by Srivastava, indicating that the Co content alters the (111) and (200) diffraction lines of the Ni-Co coating [34].

The crystalline size of the coating, as calculated by the Scherrer formula at different Co contents is summarized in Table 3. The crystalline size of the Ni-Co/hBN composite coatings changes significantly with changing Co content. The results show that there is a drop in crystalline size (from 86 nm to 24 nm) when the Co content increases from 0 wt% to 37 wt% and a slight rise (from 24 nm to 26 nm) when the Co content is further increased to 53 wt%. The crystalline size of the Ni-hBN composite coating is 3.6 times greater than that of Ni-37Co/hBN. Due to the increase in the cobalt sulfate concentration in the plating solution, the concentration of metal hydroxides such as $Co(OH)_2$ increases during the electrodeposition process. During the growth of the coating structure, the metal hydroxides

are easily adsorbed on the active center of the growth surface, which can be used as a grain refiner to reduce the coating grain size [32]. In addition, the incorporation of hBN nanoparticles is an important reason for refining the grain size of the coatings. Alizadeh [35] reported that as alumina particles were embedded in the Ni-Mo matrix, the nucleation rate increased, which resulted in the inhibition of crystal growth. A large number of hBN nanoparticles distributed uniformly in the coatings increased the nucleation rate and hence reduced the crystalline size.

Table 3. Crystalline size of Ni-Co/hBN composite coatings with different Co contents

Cobalt sulfate concentration (g/L)	Co content (wt.%)	Coatings	Crystalline size (nm)
0	0	Ni/hBN	86
10	17	Ni-17Co/hBN	40
20	32	Ni-32Co/hBN	33
30	37	Ni-37Co/hBN	24
40	40	Ni-40Co/hBN	25
50	53	Ni-53Co/hBN	26

3.3 Microhardness

The effect of the Co content on the microhardness of the coatings is shown in Figure 9. The microhardness of the coatings first increases and then decreases as the Co content increases. It reaches the highest microhardness at a Co content of 37 wt% (575 HV), which is 2.6 times that of the Ni/hBN composite coating (220 HV). The Co content has a significant effect on the microhardness of Ni-Co/hBN composite coatings. The microhardness of the Ni/hBN composite coating is lower than that of any of the Ni-Co/hBN composite coatings.

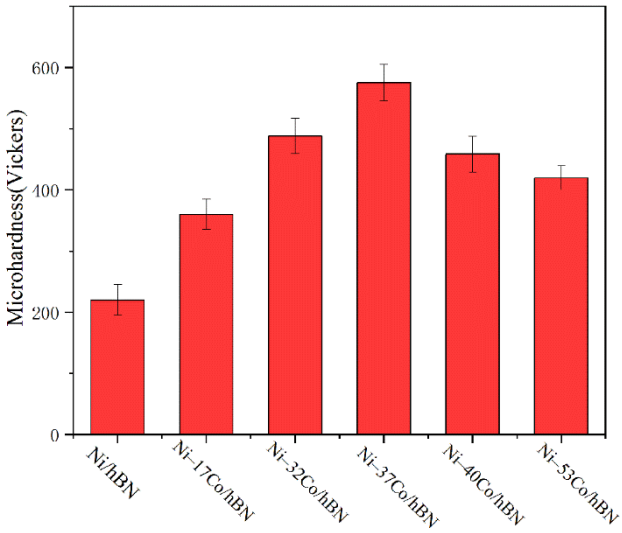

Figure 9. Microhardness of Ni/hBN, Ni-17Co/hBN, Ni-32Co/hBN, Ni-37Co/hBN, Ni-40Co/hBN and Ni-53Co/hBN nanocomposite coatings

The microhardness of the composite coatings is affected by solid solution hardening, grain refinement and reinforcing particles. The Ni-Co/hBN composite coatings improve the hardness through a solid solution hardening mechanism. On the other hand, the addition of Co and hBN reduces the grain size and the microhardness of the coatings increases according to the Hall-Petch relationship. When embedded in the form of an intercrystalline phase, hBN nanoparticles hinder plastic deformation, which improves the microhardness of the coating [36].

3.4 Corrosion resistance

The Tafel curves of Ni-Co/hBN composite coatings with different Co contents, which are carried out in a 3.5% NaCl solution, are shown in Figure 9. Table 4 lists the electrochemical parameters obtained from the Tafel curves. The Stern–Geary equation is used to calculate the corrosion current densities:

$$i_{corr} = \frac{\beta_a \cdot \beta_c}{2.303 \times R_p(\beta_a + \beta_c)} \quad (2)$$

Where i_{corr} represents the corrosion current density, β_c and β_a represent the cathodic and anodic Tafel slopes, respectively, and R_p represents the polarization resistance, which is calculated by the following equation:

$$R_p = \frac{dE}{di}|_{E=E_{OCP}} \approx \frac{\Delta E}{\Delta i} \quad (3)$$

The data extracted in Table 4 indicate that the corrosion potentials of the Ni-Co/hBN composite coatings are all higher than those of the Ni-35Co alloy coating. The corrosion current density of the coatings first decreases and then increases with increasing Co content. When the Co content increases from 0 wt% to 37 wt%, the corrosion current density of the coatings decreases from 9.093 μA/cm^2 to 0.645 μA/cm^2, a 14-fold decrease, while it rises to 6.925 μA/cm^2 as the Co content increases to 53 wt%. Compared with the coating without added hBN nanoparticles, the corrosion potentials of the Ni-Co/hBN composite coatings are higher, and the corrosion current densities are reduced.

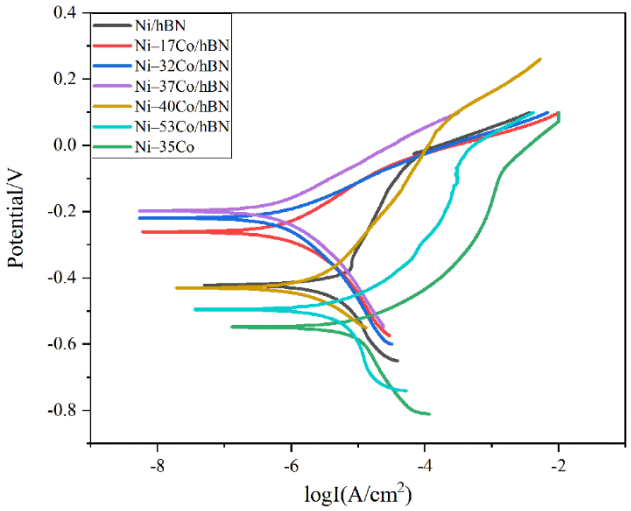

Figure 10. Tafel curves of Ni/hBN, Ni-17Co/hBN, Ni-32Co/hBN, Ni-37Co/hBN, Ni-40Co/hBN, Ni-53Co/hBN and Ni-35Co coatings

Table 4. Electrochemical data of the Ni-Co/hBN composite coatings

Coatings	Cobalt sulfate concentration (g/L)	Co content (wt.%)	E_{corr} (mV)	i_{corr} (μAcm^{-2})
Ni/hBN	0	0	-0.422	9.093
Ni-17Co/hBN	10	17	-0.261	0.916
Ni-32Co/hBN	20	32	-0.219	0.794
Ni-37Co/hBN	30	37	-0.198	0.645
Ni-40Co/hBN	40	40	-0.430	2.524
Ni-53Co/hBN	50	53	-0.495	6.925
Ni-35Co	30	35	-0.548	13.320

The corrosion resistance of the composite coating is related to the matrix, phase structure and particle properties [37]. The corrosion resistance of the Ni-Co/hBN composite coating is partly derived from the Ni-Co alloy matrix. The Ni-Co alloy has good corrosion resistance, which improves the corrosion resistance of the Ni-Co/hBN composite coatings.

According to the XRD patterns of the Ni-Co/hBN composite coatings, all of them are fcc structures. It shows that the single-phase structure has better corrosion resistance than the multiphase structure, and the fcc structure has a higher filling factor, which further improves the corrosion resistance of the Ni-Co/hBN composite coating [38].

Particle performance is an important factor affecting the corrosion resistance properties. It has been demonstrated that composite coatings containing nanoparticles have better corrosion resistance than microparticles [39]. The size of the hBN particles used in this study is approximately 50 nm, which allows them to be better incorporated into the composite coatings. During the electrodeposition process, defects such as crevices and pores will appear in the coating, which can be filled by hBN nanoparticles. In addition, from the N and B mapping images of the composite coatings, it can be seen that hBN particles are homogeneously distributed in the coatings, which will reduce the effective corrosion areas and prevent the coatings from further contacting the corrosive medium. This leads to the corrosion potential shifting in the positive direction and enhancement of the corrosion resistance of the coatings. As an insulating material, hBN has a higher standard electrode potential than the Ni-Co alloy coating. When corrosion occurs, the Ni-Co alloy can be used as the anode and hBN as the cathode, forming a large number of tiny galvanic cells, which causes the corrosion mechanism to change from local corrosion to uniform corrosion and improves the corrosion resistance of the composite coatings.

4. CONCLUSIONS

The Ni-Co/hBN composite coating was prepared by direct-current electrodeposition technology. The effects of the electrodeposition process parameters and the concentrations of hBN and Co on the composition, microhardness, surface morphology, corrosion properties and phase structure of the coatings were investigated. This study draws the following conclusions:

(1) The hBN content in the coatings first increased and then decreased as the current density and the concentrations of cobalt sulfate and hBN increased in the bath. It reached a maximum hBN content of 5.9 wt% in the coating at a deposition current density of 3 A/dm^2, cobalt sulfate concentration of 30 g/L and hBN concentration of 5 g/L.

(2) The surface morphology of the Ni-Co/hBN coatings changed gradually from pyramidal to spherical as the Co content increased. The hBN nanoparticles were homogeneously distributed in the coatings.

(3) The phase structure of the coatings did not change with changing Co content. All of the structures were fcc structures, but the preferred orientation changed. The crystalline size of the Ni-Co/hBN composite coatings first decreased and then increased with increasing Co content, with a minimum value of 24 nm.

(4) The microhardness of the coatings first increased and then decreased. Ni-37Co/hBN had the highest value of 575 HV, which was related to the solid solution strengthening of the Ni-Co alloy matrix and the addition of hBN particles.

(5) The corrosion potentials of the Ni-Co/hBN composite coatings were higher than that of the Ni-35Co alloy coating, but the corrosion current densities were the opposite. The Ni-37Co/hBN composite coating had the lowest corrosion current density value of 0.645 μA/cm^2. The corrosion resistance of the coatings was related to the phase structure, matrix and particle properties.

ACKNOWLEDGMENT
This study was supported by the Key Project of Shaanxi Province Science and Technology (2016NY-137).

CONFLICT OF INTEREST
The authors declare that there are no conflicts of interest.

References

1. G.-C. Son, D.-K. Hwang, J. Jang, S.-S. Chee, K. Cho, J.-M. Myoung and M.-H. Ham, *Nano Res.,* 12 (2018) 19.
2. D. He, S. Zheng, J. Pu, G. Zhang and L. Hu, *Tribol. Int.,* 82 (2015) 20.
3. Y. Yu, Y. Li, H. Qin and X. Cheng, *Mater. Des.,* 196 (2020) 109151.
4. S. I. Ghazanlou, A. Shokuhfar, S. Navazani and R. Yavari, *Bull. Mater. Sci.,* 39 (2016) 1185.
5. M. S. Safavi, F. Babaei, A. Ansarian and I. Ahadzadeh, *Ceram. Int.,* 45 (2019) 10951.
6. V. Torabinejad, M. Aliofkhazraei, S. Assareh, M. H. Allahyarzadeh and A. S. Rouhaghdam, *J. Alloys Compd.,* 691 (2017) 841.
7. S. Khorsand, K. Raeissi, F. Ashrafizadeh, M. A. Arenas and A. Conde, *Appl. Surf. Sci.,* 364 (2016) 349.
8. B. Li, W. Zhang, W. Zhang and Y. Huan, *J. Alloys Compd.,* 702 (2017) 38.
9. J. H. Liu, W. H. Li, Z. L. Pei, J. Gong and C. Sun, *Mater. Charact.,* 167 (2020) 110532.
10. N. Elkhoshkhany, A. Hafnway and A. Khaled, *J. Alloys Compd.,* 695 (2017) 1505.
11. M. Demir, E. Kanca and İ. H. Karahan, *J. Alloys Compd.,* 844 (2020) 155511.
12. Y. Deo, S. Guha, K. Sarkar, P. Mohanta, D. Pradhan and A. Mondal, *Appl. Surf. Sci.,* 515 (2020) 146078.
13. U. K. Chanda, S. P. Padhee, A. K. Pandey, S. Roy and S. Pati, *Int. J. Hydrogen Energy,* 45

(2020) 21892.
14. M. S. Safavi, M. Tanhaei, M. F. Ahmadipour, R. G. Adli, S. Mahdavi and F. C. Walsh, *Surf. Coat. Technol.*, 382 (2020) 125153.
15. A. Karimzadeh, M. Aliofkhazraei and F. C. Walsh, *Surf. Coat. Technol.*, 372 (2019) 463.
16. A. Karimzadeh, A. S. Rouhaghdam, M. Aliofkhazraei and R. Miresmaeili, *Tribol. Int.*, 141 (2020) 105914.
17. A. Hefnawy, N. Elkhoshkhany and A. Essam, *J. Alloys Compd.*, 735 (2018) 600.
18. S. I. Ghazanlou, S. Ahmadiyeh and R. Yavari, *Surf. Eng.*, 33 (2017) 337.
19. W. Jiang, L. Shen, M. Xu, Z. Wang and Z. Tian, *J. Alloys Compd.*, 791 (2019) 847.
20. A. Rasooli, M. S. Safavi and M. K. Hokmabad, *Ceram. Int.*, 44 (2018) 6466.
21. B. Li and W. Zhang, *J. Alloys Compd.*, 820 (2020) 153158.
22. S. I. Ghazanlou, A. H. S. Farhood, S. Ahmadiyeh, E. Ziyaei, A. Rasooli and S. Hosseinpour, *Metall. Mater. Trans. A*, 50 (2019) 1922.
23. Y. W. Phuan, M. N. Chong, K. Egamparan, B. K. Lee, T. Zhu and E. S. Chan, *J. Taiwan Inst. Chem. Eng.*, 66 (2016) 249.
24. H. A. Murdoch, E. Hernández-Rivera, A. Thornton, D. Yin and A. K. Giri, *Scr. Mater.*, 188 (2020) 212.
25. Z. Li, K. Hu, M. Yang, Y. Zou, J. Yang, M. Yu, H. Wang, X. Qu, P. Tan, C. Wang, X. Zhou and Z. Li, *Nano Energy*, 58 (2019) 852.
26. S. I. Ghazanlou, A. H. S. Farhood, S. Hosouli, S. Ahmadiyeh and A. Rasooli, *Mater. Manuf. Processes*, 33 (2017) 1067.
27. C. Ma, D. Zhao and Z. Ma, *Ceram. Int.*, 46 (2020) 12128.
28. P. R. Dheeraj, A. Patra, S. Sengupta, S. Das and K. Das, *J. Alloys Compd.*, 729 (2017) 1093.
29. S. I. Ghazanlou, A. H. S. Farhood, S. Hosouli, S. Ahmadiyeh and A. Rasooli, *J. Mater. Sci.: Mater. Electron.*, 28 (2017) 15537.
30. E. Ünal and İ. H. Karahan, *Surf. Coat. Technol.*, 333 (2018) 125.
31. A. D. Pingale, S. U. Belgamwar and J. S. Rathore, *Bull. Mater. Sci.*, 43 (2020) 66.
32. B. Bakhit, *Surf. Coat. Technol.*, 275 (2015) 324.
33. B. Bakhit and A. Akbari, *J. Coat. Technol. Res.*, 10 (2013) 285.
34. M. Srivastava, V. E. Selvi, V. K. W. Grips and K. S. Rajam, *Surf. Coat. Technol.*, 201 (2006) 3051.
35. M. Alizadeh and A. Cheshmpish, *Appl. Surf. Sci.*, 466 (2019) 433.
36. Z. Shahri and S. R. Allahkaram, *Trans. Nonferrous Met. Soc. China*, 23 (2013) 2929.
37. Z.-w. Jia, W.-c. Sun, F. Guo, Y.-r. Dong and X.-j. Liu, *RSC Adv.*, 8 (2018) 12138.
38. O. S. Adesina, B. A. Obadele, G. A. Farotade, D. A. Isadare, A. A. Adediran and P. P. Ikubanni, *J. Alloys Compd.*, 827 (2020) 154245.
39. B. Li, W. Zhang and D. Li, *J. Alloys Compd.*, 821 (2020) 153258.